Running Title : Distraction and control effects on pain

Distraction and cognitive control independently impact parietal and prefrontal response to pain

Nicolas Silvestrini[1] & Corrado Corradi-Dell'Acqua[2,3]

[1]Geneva Motivation Lab, Faculty of Psychology and Educational Sciences, University of Geneva, Switzerland

[2] Theory of Pain Lab, Faculty of Psychology and Educational Sciences, University of Geneva, Switzerland

[3] Geneva Neuroscience Center, University of Geneva, Switzerland

Original article,
Title, 95 characters (including spaces)
Running title: 39 characters (including spaces)
Main Text: 4974 words (excluding references, legends and acknowledgments)
6 figures
3 Tables

We have no relevant conflicts of interest to declare.

Mailing Address: Nicolas Silvestrini
Dpt. of Psychology, UNI-MAIL, 40, boulevard du Pont d'Arve
CH-1205 Geneva, Tel: +41 22 379 92 68
Email : nicolas.silvestrini@unige.ch

Corrado Corradi-Dell'Acqua
Campus Biotech, 9 Chemin des Mines
CH-1211 Geneva, Tel: +41 22 379 0958
Email : corrado.corradi@unige.ch

Abstract

Previous studies found that distracting someone through a challenging activity leads to hypoalgesia, an effect mediated by parietal and prefrontal processes. Other studies suggest that challenging activities affect the ability to regulate one's aching experiences, due to partially-common neural substrate between cognitive control and pain at the level the medial prefrontal cortex. We pulled apart effects of distraction and cognitive control on pain by delivering noxious stimulations *During* or *After* (factor TIMING) a Stroop paradigm (requiring high cognitive load) or a neutral condition (factor TASK). We found that TIMING influenced subjective pain experience, with less intense and unpleasant ratings *During* task execution. This hypoalgesia was associated with enhanced activity at the level of the dorsolateral prefrontal cortex and the posterior parietal cortex, in interaction with the insula. Furthermore, multivariate pattern analysis revealed that distraction altered the neural response to pain, by making it more similar to that associated with previous Stroop tasks. All these effects were independent of the nature of the TASK which, instead, led to a localized neural modulation around the anterior cingulate cortex. Overall, our study underscores the role played by two facets of human executive functions, which exert independent influence in the neural response of pain.

Keywords: Stroop, Attention, connectivity, cingulate, insula

Introduction

Previous studies established that pain engages and interacts with high-level executive functions (Tracey and Mantyh, 2007; Bushnell *et al.*, 2013; Wiech, 2016). For instance, distracting someone through a concurrent activity might decrease one's sensitivity to pain (Petrovic *et al.*, 2000; Tracey *et al.*, 2002; Valet *et al.*, 2004; Buhle and Wager, 2010). At the neural level, distraction hypoalgesia has been associated with decreased activity in regions often implicated in pain processing, such as somatosensory and insular cortices (Petrovic *et al.*, 2000; Valet *et al.*, 2004; Seminowicz and Davis, 2007b), but also with enhanced signal within the prefrontal cortex (Petrovic *et al.*, 2000; Valet *et al.*, 2004) and periaqueductal gray (Tracey *et al.*, 2002; Valet *et al.*, 2004). Overall, these effects have been interpreted consistently with the neurocognitive model of attention to pain according to which bottom-up nociceptive inputs can engage one's attention, but do so in competition with top-down processes, such as prefrontal and parietal mechanisms for maintaining attentional load and the processing of goal-relevant stimuli (top-down attention) (Legrain *et al.*, 2009).

Despite the overall consensus, several considerations put into question the role played by distraction on pain sensitivity. On the one side, some studies failed to replicate the effect (McCaul *et al.*, 1992; Duker *et al.*, 1999) or, at least, limit its efficacy to a subgroup of individuals (Keogh *et al.*, 2000; Seminowicz *et al.*, 2004; Nouwen *et al.*, 2006; see also Seminowicz and Davis, 2007a). On the other side, distraction is often manipulated by delivering pain *During* the execution of highly demanding tasks (e.g., Stroop, N-Back) which, however, exert extensively individual control/regulatory processes by asking to select an appropriate response among multiple

competing information. Cognitive control might influence pain experience independently of distraction, as suggested by studies describing changes in the sensitivity to pain delivered *After* a Stroop task (Silvestrini and Rainville, 2013; Hoegh *et al.*, 2019; Silvestrini *et al.*, 2020) compared to a neutral (easier) activity. Furthermore, pain and cognitive control disclose distinct but co-localized neural networks (Kragel *et al.*, 2018; Silvestrini *et al.*, 2020), which are integrated at the level of the medial prefrontal cortex (Shackman *et al.*, 2011; Silvestrini *et al.*, 2020), partly reminiscently of the neural structures held to mediate distraction hypoalgesia. It is view, it is unclear to whether (and to which extent) effects of distraction on pain are partly confounded by those of cognitive control. Partial evidence in favour of the independence of the two processes arises by studies modulating parametrically the cognitive load of the distracting task, who failed to find a consequent linear influence on pain sensitivity (Hodes *et al.*, 1990; McCaul *et al.*, 1992; Seminowicz and Davis, 2007b). However, to the best of our knowledge, the effects of distraction and cognitive control on the behavioural and neural response pain have never been pulled apart completely.

We run an experiment where we administered noxious thermal stimulations either *During* or *After* (factor TIMING) an interfering Stroop (with high control load) or an easier neutral paradigm (factor TASK), whilst recording pain-related ratings and neural response through fMRI. We predicted that pure effects of distraction should be observed when pain was administered *During* a task (regardless of its cognitive demands), with associated modulations at the level of prefrontal-parietal structures. Instead, pure effects of cognitive control should be observed when comparing the Stroop task *vs*. the Neutral condition. The critical question, however, is whether

TIMING and TASK influence pain experience independently, or whether instead they interact with one another.

Methods

Participants and Design

Twenty-nine participants (11 males, mean age = 23.86 ± 4.75 SD) were recruited for the experiment. Participants were free of self-reported acute or chronic pain, and cardiovascular, neurological, or psychological disease. They signed an informed consent prior to the experiment. This research was conducted in accordance with the Declaration of Helsinki and was approved by the local ethical committee.

Painful Thermal Stimulation

A computer controlled thermal stimulator with a 25 x 50 mm fluid-cooled Peltier probe (MSA Thermotest, Somedic, Hörby, Sweden) delivered painful thermal stimulations. The baseline temperature was set to 36°C and each stimulation lasted 16 sec (3 sec of temperature increase, 10 sec of plateau, and 3 sec of temperature decrease). The temperature of the painful stimulations was adjusted for each participant using a calibration procedure.

fMRI Data Acquisition

A Siemens Trio 3-T whole-body scanner was used to acquire both T1-weighted anatomical images and gradient-echo planar T2*-weighted MRI images with blood oxygenation level dependent (BOLD) contrast. Structural images were acquired with a T1-weighted 3D sequence (repetition time = 1900 msec, inversion time = 900 msec, echo time = 2.27 msec, 1 × 1 × 1 mm voxel size).

The functional sequence was a trajectory-based reconstruction sequence with a repetition time (TR) of 2100 msec, an echo time (TE) of 30 msec, a flip angle of 90 degrees, in-plane resolution 64x64 voxels (voxel size 3 x 3 mm), 32 slices, a slice thickness of 3 mm, and no gap between slices.

Experimental Paradigm

Before the scanning session, participants were seated in front of a desktop computer. The probe of the thermal stimulator was installed on their right leg in the lower part of the shinbone and the individual painful temperature was identified through staircase procedure. Specifically, we applied three series of ascending and descending thermal stimulations. Participants rated the pain unpleasantness of each stimulation with a visual analogue scale (VAS) ranging from 0 (*Not unpleasant at all*) to 100 (*The most unpleasant pain imaginable*). After an initial increase by steps of 2°C, the temperature started decreasing when participants rated pain unpleasantness as more than 70 and increased again when pain unpleasantness was lower than 50. The last series of ascending and descending stimulations included steps of 1°C. Based on participants' ratings, we selected a temperature that elicited a pain unpleasantness response of about 70 (temperature: M = 47.07, SD = 1.83, range = 42-51). The selected temperature remained constant throughout the subsequent scanning experiment. This approach was comparable to the one used in our previous research (Silvestrini and Corradi-Dell'Acqua, 2022) and was motivated by the fact that, under a similar set-up, unpleasantness assessments were associated with stronger effect sizes than intensity ratings (Silvestrini *et al.*, 2020).

Then, participants were engaged in a practice session for the same Stroop paradigm from previous research (Silvestrini and Rainville, 2013; Silvestrini *et al.*, 2020; Silvestrini and Corradi-Dell'Acqua, 2022). Specifically, they were exposed to sets of one-to-four identical words

presented vertically on the screen. They were asked to report the number of words displayed (regardless of their meaning) as quickly/accurately as possible, with an emphasis placed on not sacrificing accuracy for speed. Moreover, participants were asked not to blur their vision preventing them to read effortlessy the words. In the interference condition, the words used was one of “one”, “two”, “three”, and “four” (in French, “un”, “deux”, “trois”, “quatre”), so that it was always inconsistent with the correct response. In the neutral condition, we used instead words of matched length which were not held to elicit any interference: “year”, “sheet”, “table”, and “skittle” (in French, “an”, “drap”, “table”, and “quille”). Words were presented in capital letters in the font Verdana size 24. Trials started with a fixation cross (750ms) followed by the words which stayed on the screen until a response was delivered (but never more than 1250ms). During this practice session, participants received also feedback about their proficiency and speed.

Subsequently, participants were installed on the scanner bed, where they underwent two functional runs of 21 min each, separated by the anatomical scan. Both scanning runs began with a painful thermal stimulation used as a baseline pain induction. After the stimulation, participants rated pain and unpleasantness felt using a cursor displayed on the screen over two VAS and controlled with the middle and index fingers. The scales ranged from *No pain/Not unpleasant at all* (0) to *The most intense/unpleasant pain imaginable* (100). Then participants performed four blocks of the Stroop task. However, differently from the practice session, the feedback provided was uninformative of one’s performance. The feedback appeared for 2 sec minus participants’ reaction time, assuring that all trials (3.4 sec) had the same length. Inter-trial intervals varied randomly (750-1500 ms). In the *During* condition, the blocks included 36 trials (2 min 30 sec) and

a thermal stimulation was administered at the 32nd trial while the participants were performing the remaining four trials. In the *After* condition, the blocks included 32 trials (2 min) and a stimulation was administered right after the end of the task. Each run included the four possible blocks (*During/Interference*, *After/Interference*, *During/Neutral*, and *After/Neutral*), which were separated by a short break of 12 sec. The order of the blocks was counterbalanced within the runs. At the end of the task and stimulation, participants rated pain and unpleasantness associated with the thermal event (total rating time allowed: 24sec) and one item of perceived task difficulty ("How difficult was it for you to achieve the task successfully?"; *Not at all* [0] to *Very difficult* [10]).

Visual and thermal stimuli were delivered using Eprime 2.0 Software (Psychology Software Tools Inc., Pittsburgh, PA, USA). Images were displayed on a computer monitor back projected onto a screen and viewed on a mirror placed on the head coil.

Data Processing

Behavioural Data

For each subject and condition, the average Accuracy and correct Reaction Times from Stroop trials were fed to a paired-sample t-test probing differences between Interference *vs*. Neutral TASK conditions. As for participants' subjective ratings, average Intensity and Unpleasantness values were analysed with Repeated Measures ANOVA, with TIMING (*During vs. After*) and TASK (*Interference vs. Neutral*) as within-subject factors. The analysis was run using R 4.0.4 software (http://cran.r-project.org).

Imaging processing

Preprocessing. Statistical analysis was performed using the SPM12 software (http://www.fil.ion.ucl.ac.uk/spm/), exploiting the preprocessing pipeline from the CONN 21 toolbox (https://web.conn-toolbox.org/, Whitfield-Gabrieli and Nieto-Castanon, 2012). For each subject, functional images were realigned to correct for head-movement artefacts, unwrapped to account for geometric distortions related to the magnetic field inhomogeneity, and slice-time corrected to account for temporal delays within the acquisition of a whole brain volume. The Artifact Detection Tools, embedded in the CONN toolbox, were then used for identification of outlier scans in terms of excessive subject motion and signal intensity spikes. Finally, the images were then normalized to a template based on 152 brains from the Montreal Neurological Institute (MNI) with a voxel-size resolution of 2 x 2 x 2 mm, and smoothed by convolution with an 8 mm full-width at half-maximum Gaussian kernel.

First-Level analysis. Preprocessed images from each task were analysed using the General Linear Model (GLM) framework implemented in SPM. For each functional run, we modelled the onset of each of the five thermal stimulations of interest (4 main condition + baseline) with a boxcar function of 10 sec duration starting the moment in which thermode reached the plateau temperature. As for the Stroop task, each of the two conditions (*Interference* and *Neutral*) was delivered through ~2 minutes blocks. Although optimal for testing cognitive control after-effects on pain (Silvestrini and Rainville, 2013; Silvestrini *et al.*, 2020), such long block structure poorly accords with default filtering in SPM (128 sec). To circumvent this, we modelled the onset of each Stroop trial (without distinguishing between *Interference* and *Neutral* blocks) as a delta function, and added an additional predictor of interest in which trials Reaction Times were modulated parametrically. This predictor is expected to capture both differences between Interference and

Neutral Stroop blocks (see results) and within-block fluctuations in performance, and represents a reliable test for neural responses of cognitive control which is not confounded with signal low-frequency noise/drifts. This led to 7 predictors for each functional run (5 thermal stimulations, 1 Stroop, 1 Reaction Times parametrical modulation), which were convolved with a canonical hemodynamic response function and associated with their first order temporal derivative. To account for movement-related variance, and other sources of noise, we included the differential movement parameters from the realignment, and dummy variables signalling outlier scans (from the ART toolbox) as covariates of no interest. Low-frequency signal drifts were filtered using a cut-off period of 128 sec, and serial correlation in the neural signal were accounted through first-order autoregressive model AR(1).

Second-level Analyses. Functional contrasts, testing differential parameter estimates images associated with one experimental condition *vs.* the other were then fed in a second level one-sample t-test using random-effect analysis. Effects were identified as significant only if they exceeded a FWE cluster-level correction for multiple comparisons at the whole brain (Friston *et al.*, 1993), with an underlying voxel-level threshold corresponding to $p < 0.001$ (uncorrected).

Functional Connectivity. Preprocessed images were denoised through the default pipeline in CONN toolbox to remove components in the neural signal which were related to (1) white matter and cerebro-spinal fluid signal (first 15 principal components), (2) estimated subject movement parameters (from preprocessing), (3) the presence of outlier scans (estimated through the ART toolbox during preprocessing), and (4) task-related BOLD signals (in our case, pain-evoked activity and stroop trials). Data was also band-pass filtered (0.008-0.09 Hz) to account both for slow-frequency fluctuations (such as scanner drift) and well as physiological and

residual movement artefacts. Subsequently, denoised data was fed to ROI-to-ROI connectivity analysis using generalized psychophysiological interaction (gPPI) (McLaren *et al.*, 2012). For the purpose of this analysis we considered the ROIs from Brainnetome parcellation of the human brain (Fan *et al.*, 2016). This allows for a whole-brain fine-grain exploration of the regions involved without any a priori assumption on the implicated network. In particular, we focused on 224 ROIs comprehending the whole atlas, except for the regions 189-210 corresponding to the occipital cortex (Fan et al., 2016, Table 1) which were outside our range of interest. gPPI is a task-dependent connectivity analysis computing how strongly the BOLD response time course of two regions are coupled in a given condition (in our case, thermal stimulations). This is implemented though a regression model, whereby the time course of target ROIs is regressed against that of a seed ROI multiplied with the psychological variable. Within the network of interest, every possible combination of seed-target ROIs was considered, thus leading to a 224 x 224 regression coefficients (βs) matrix for each participant and condition. For group-level analysis, individual βs were converted to *z*-scores with Fisher's transformation. Functional contrasts, testing coupling parameters associated with one experimental condition *vs.* the other were then fed in a second level random-effect analysis. To identify conditions of interest, we applied Spatial Pairwise Clustering correction (Zalesky *et al.*, 2012), as implemented in the CONN 21 toolbox. This approach is reminiscent to the cluster-based correction for multiple comparisons for fMRI activation: in this case regression coefficients are clustered together based on hierarchical cluster analysis based on both functional and spatial criteria (weighting factor 0.5). The cluster mass of connections exceeding a height threshold corresponding to $p < 0.01$ (uncorrected) was validated statistically based on the null distribution of obtained through 1000 permutations of the original

dataset. In particular, clusters were identified as significant if exceeding FDR correction at $p < 0.05$.

Multivariate Pattern Analysis. We also fed the data to multivariate models predictive of subjective pain from brain activity estimated on independent datasets. More specifically, we choose the model from Sharvit *et al.* (2020). This model was obtained through non-linear Support Vector Regression on data obtained with the same thermal device and MRI scanner than the present study, and validated both within the sample used for the estimation (through cross-validation) and across different cohorts (Sharvit *et al.*, 2020). Brain-based estimations of pain unpleasantness from this model were obtained through the code available under the Open Science Framework at https://osf.io/jkrvp/, and were originally coded in a scale ranging from 0 (neutral) to 50 (extremely unpleasant) (Sharvit *et al.*, 2020). To improve compatibility with the present study, this output was recoded in a 0-100 scale. This model of pain unpleasantness (Sharvit *et al.*, 2020) was applied to pain-evoked parameter estimates in each subject, session and condition. The resulting estimates were then fed to the same ANOVA scheme used for behavioural measures.

We also considered a multivariate whole-brain model predictive of high (*vs*. low) demands in a Stroop task developed by Silvestrini *et al.* (2020), obtained through linear Support Vector Classification. The brain-based estimation of Stroop demand was obtained through the code available at the following repository: https://github.com/canlab/Neuroimaging_Pattern_Masks/tree/master/Multivariate_signature_patterns/. This model was used as sanity check to assess whether it could predict Stroop-evoked activity in our data. For this specific case, we created an *ad hoc* first-level model where we

modelled the trials with longest responses in each session separately from those with the most rapid reactions (through median split). We then applied both models to the parameter estimates associated with Long and Short Reaction Times and assessed potential differences in the output through paired sample t-test.

Results

Behavioural Responses

Stroop performance

We confirmed that participants were both less accurate (95% *vs*. 94%, $t_{(28)}$ = -2.32, p = 0.028, Cohen's d = -0.44) and slower at responding correctly (629.47 *vs*. 649.34 ms, $t_{(28)}$ = 4.48, p < 0.001, d = 0.83) during the Interference, as opposed to the Neutral condition (see Figure 1A-B).

Thermal Ratings

We analysed thermal ratings through an ANOVA, which revealed a main effect of TIMING (Pain Intensity: $F_{(1,28)}$ = 7.88, p = 0.014, η_p^2 = 0.22; Unpleasantness: $F_{(1,28)}$ = 6.25, p = 0.018, η_p^2 = 0.19). In particular, individuals felt painful temperatures as less intense (69.02 vs. 71.84) and unpleasant (66.17 *vs*. 69.01) *During* the task, rather *After* its completion (see Figure 1C-D). No significant modulation of TASK was found, neither as main effect nor in interaction with TIMING ($F_{(1,28)}$ ≤ 1.40, p ≥ 0.246). Overall, our data confirm previous evidence of distraction-based hypoalgesia, whereby individuals consider pain less intense and unpleasant while actively engaged in a task.

Neural Responses

Stroop performance

We ran a linear regression searching for regions whose activity increased monotonically with the Reaction Times. Consistently with a wide range of studies employing Stroop (Laird *et al.*, 2005; Hung *et al.*, 2018), and other tasks involving cognitive control (Shackman *et al.*, 2011; Hung *et al.*, 2018; Kragel *et al.*, 2018), we implicated a wide network involving the middle cingulate cortex, supplementary motor area, precuneus, anterior insula (AI), dorsolateral prefrontal cortex (DLPFC), posterior parietal cortex (PPC), thalamus, etc (see Table 1 and Figure 2A for more

details). To gather a more stringent functional interpretability of this network, we took a model-based approach, and fed our dataset to a predictive model of Stroop high (*vs*. low) demand developed on an independent dataset (Silvestrini *et al.*, 2020). When applied to our data, we confirmed that this model led to a much stronger output for Stroop trials with longer Reaction Times, than those processed rapidly ($t_{(28)} = 5.07$, $p < 0.001$, $d = 0.94$; see Figure 2B). Instead, when feeding the same data to whole-brain models predictive of pain unpleasantness (Sharvit *et al.*, 2020) we found no differential output between long vs. short Reaction Times in Stroop ($t_{(28)} = 0.69$, $p = 0.497$, $d = 0.13$; see Figure 2C). Overall, the activity patterns evoked by Stroop demands appear to be similar to that of previous tasks testing cognitive control via Stroop (Silvestrini *et al.*, 2020), while at the same time they differ from those implicated in thermal pain (Sharvit *et al.*, 2020).

Baseline Pain

Subsequently, we inspected the neural responses associated with the delivery of painful temperatures. Figure 3A and Table 2 report brain-evoked activity by the baseline stimulation introducing each experimental session (relative to the non-specified parts of the model [implicit baseline]), and confirm a widespread network involving bilateral operculum, insula (in both posterior and anterior portions), PPC and right inferior frontal gyrus.

Finally, we fed the brain activity evoked by the baseline temperatures with the whole-brain model predictive of pain unpleasantness (Sharvit *et al.*, 2020), and found a stronger output for those subjects/sessions in which pain was delivered through a higher temperature (Pearson's $r = 0.46$, $p = 0.013$; Figure 3B). Please note that the temperature was optimized at the individual level to account for individual differences in pain sensitivity, and that these differences in

nociceptive intensity were reliably captured by this pain model. Interestingly, when feeding the same data to a whole brain model for Stroop demands (Silvestrini *et al.*, 2020), a similar positive relationship between predicted outcome and stimulation temperature was observed ($r = 0.44$, $p = 0.017$; Figure 3B). Hence, although pain and cognitive control activity patterns dissociate at the neural level (Kragel *et al.*, 2018; Silvestrini *et al.*, 2020), it is possible to observe the occurrence of both in the neural response evoked by painful stimulations (Silvestrini *et al.*, 2020).

Stroop-related Pain

Effects of distraction. We then tested the degree to which pain-evoked activity was influenced by the Stroop task. More specifically, when analyzing the main effect of TIMING, we found stronger activity *During* (*vs. After*) the Stroop task in the bilateral DLPFC, bilateral PPC and middle temporal gyrus. Further activity was observed at the level of the dorsomedial prefrontal cortex (Figure 4A and Table 2). No region displayed stronger activity in the *After* (vs. *During*) condition. We analyzed the effect of TIMING also from a connectivity point of view. This analysis identified three clusters of connections similarly impacted by the presence of the Stroop task. In particular, we found that the right and left PPC exhibited decreased connectivity with right DLPFC and AI (Figure 4A, green tracks). Additionally, we also found that the right DLPFC showed increased connectivity with the cingulate cortex, in both its' dorsal (dACC) and subgenual aspects (Figure 4A, purple tracks).

Effects of Stroop demands. Subsequently, we analyzed the effect played by TASK in pain-evoked activity, both as a main effect and in interaction with TIMING. When applying rigorous correction for multiple comparisons for the whole brain no effects were observed. However, under a less conservative threshold (corresponding to $p < 0.001$ uncorrected), we found the

dorsal anterior cingulate cortex (dACC) implicated in the main effect of TASK (x = 12, y = 38, z = 20, $t_{(28)}$ = 4.50, p < 0.001 uncorrected, 122 consecutive voxels), with stronger activity when pain was associated to the Interference (*vs*. Neutral) Stroop condition (Figure 5). No effect was associated with the TASK*TIMING interaction. Finally, no effects of Stroop demands were found at the level of connectivity, neither when testing the TASK main effect, nor when modelling the TASK*TIMING interaction

Multivariate Patterns. To achieve a more reliable functional interpretation of our results, we fed the pain-evoked response to a whole-brain model predictive of pain unpleasantness (Sharvit *et al.*, 2020) and Stroop demands (Silvestrini *et al.*, 2020). More specifically, we analyzed the models' output through the same ANOVA scheme used for subjective ratings. For both models we found a main effect of TIMING (Pain Unpleasantness: $F_{(1,28)}$ = 8.74, p = 0.006, η_p^2 = 0.24; Stroop Demands: $F_{(1,28)}$ = 5.53, p = 0.026, η_p^2 = 0.17). Figure 6 displays the models' output across the different conditions and reveal that, consistently with what found for subjective responses, brain-estimates of Pain Unpleasantness decreased *During vs. After* the task. Instead, brain estimates of Stroop demands during pain showed an opposite trend, as they increased when participants were engaged in the task, rather than subsequent to it. No significant effects were associated with the factor TASK, neither as main effect, nor in interaction with TIMING ($F_{(1,28)}$ ≤ 1.17, p ≥ 0.289).

Discussion

We found a functional dissociation in the role played by distraction and cognitive control in pain experience. Participants rated pain as less intense and unpleasant while they were engaged in an active task, consistently with previous research on distraction hypoalgesia (Petrovic *et al.*, 2000; Tracey *et al.*, 2002; Valet *et al.*, 2004; Buhle and Wager, 2010). Such effect was associated with an increased activity at the level of prefrontal, parietal and temporal structures, but also by negative connectivity between the PPC and DLPFC-AI. Finally, multivariate pattern analysis revealed that distraction altered the neural pain response, by making it less similar to that usually observed during thermal stimulations (Sharvit *et al.*, 2020), and more aligned to that associated with Stroop (Silvestrini *et al.*, 2020). Critically, all these effects were observed independently of cognitive control demands of the TASK employed which, instead, led to a selective increase of neural activity around dACC.

Distraction and pain response

Our findings nicely dovetail the predictions from the neurocognitive model of attention to pain (Legrain *et al.*, 2009), which speculates that PPC is associated with individual attentional set, including maintaining the focus on goal-relevant stimuli while inhibiting information from competing sources of information. In line with the prediction of this model, we found increased PPC activity *During* task execution (Figure 4A), and its' negative coupling with AI (Figure 4B). This possibly reflects an inhibitory mechanism which, in turn, can explain previous evidence of decreased insular activity associated with distraction hypoalgesia (Petrovic *et al.*, 2000; Valet *et al.*, 2004; Seminowicz and Davis, 2007b). In this view, multiple studies showed how AI plays a key role in pain appraisal, by integrating bottom-up nociceptive signals with top-down factors related

to attention and expectation (Atlas *et al.*, 2010; Geuter *et al.*, 2017; Fazeli and Büchel, 2018; Sharvit *et al.*, 2018). It is therefore likely that the PPC-AI inhibition observed here might nullify these top-down influences, by making one's sensitivity more dependent on incoming ascending inputs.

Consistently with previous research, we also found that distraction increased activity at the level of the lateral and medial prefrontal cortex (Petrovic *et al.*, 2000; Valet *et al.*, 2004). Interestingly, however, connectivity analysis suggests that DLPFC activity is highly coupled with that of AI, but negatively associated with PPC. It is possible that, differently from PPC, DLPFC underlies compensatory processes which are engaged whenever the signal in structures like AI is high. This interpretation would fit the neurocognitive model of attention to pain which speculates that DLPFC is implicated in maintaining attentional load towards the main task (Legrain *et al.*, 2009), a process that could be recruited in larger extent the more competing pain signals are strong.

As for the medial portions of the prefrontal cortex, this region could play a key role triggering descending regulatory mechanisms for pain at the level of striatum, periaqueductal grey and spinal cord (Valet *et al.*, 2004; Sprenger *et al.*, 2015; Woo *et al.*, 2015; Tinnermann *et al.*, 2017). These pathways have been partly observed in previous research on distraction (Petrovic *et al.*, 2000; Tracey *et al.*, 2002; Valet *et al.*, 2004), thus associating hypoalgesia to a well-known neurobiological model of pain regulation. In principle, the same processes could be at play also in our research, although we found no evidence that medial prefrontal cortex was interacting with the midbrain during distraction.

Cognitive Control and pain response

When analysing the effects of TASK we found enhanced pain responses in dACC associated with an interfering Stroop (vs. neutral control), regardless of whether this condition preceded or was concurrent to the pain stimulation (Figure 5). These results fit previous findings who identify dACC as a key hub for the interplay between cognitive control and pain (Shackman *et al.*, 2011; Silvestrini *et al.*, 2020). Importantly, although neural effects of cognitive control are orthogonal to those associated with distraction, they might not be independent from them as dACC exhibits also enhanced connectivity with DLPFC-AI during task execution. Hence, pain responses in dACC are also influenced by the attentional manipulation, possibly reflecting some degree of overlap between these two facets of human executive functions.

Behaviourally we found no effect of Stroop-induced cognitive control on participants' pain sensitivity. This might appear at odds with the literature who found significant modulations, albeit with different directions (Silvestrini and Rainville, 2013; Hoegh *et al.*, 2019; Silvestrini *et al.*, 2020). It is reasonable to assume that hidden moderators/confounds might have influenced previous and current results. For instance, we recently found that cognitive control after-effects in pain are influenced by the intensity of the noxious input, with mild stimulations associated with hyperalgesia but more intense events with hypoalgesia (Riontino *et al.*, 2022). Although it is difficult to compare the present study to others who used different parameters, it is possible that the stimulation adopted here fell within a "medium" range where its' susceptibility to cognitive control manipulations was minimum. Future studies will need to further investigate the effect of cognitive control and pain sensitivity.

Limitations of the study and conclusive remarks

Given the nature of the research question, our experimental design was constrained by long task sessions (Silvestrini and Rainville, 2013; Silvestrini *et al.*, 2020), each associated with one thermal stimulation. This made the task-related signal susceptible to low-frequency fluctuations (which was accounted for in the analysis), whereas pain-related activity was based on limited repetitions, and with no room for a control painless stimulation. Finally, Figure 1C-D shows a strong desensitization between the first (baseline) thermal stimulation and the subsequent ones. We believe that these limitations have little impact on the main conclusions of the study, which proved to be sufficiently sensitive to capture strong thermal-related increases in the neural signal, and associated attentional effects. Furthermore, the neural modulations associated with TIME mirrored closely behavioural measures of pain and unpleasantness. As for the TASK manipulation, it is possible that the lack of positive behavioural effects might reflect its poor effectiveness at influencing pain response, although the same design was effectively used to document positive influences of Stroop on pain (Silvestrini and Rainville, 2013; Silvestrini *et al.*, 2020) and vice versa (Silvestrini and Corradi-Dell'Acqua, 2022).

Keeping these limitations aside, in this study we pulled apart the role of distraction and cognitive control in pain, with the former affecting subjective experience and triggering a widespread network involving PPC and DLPFC in interaction with AI, and the latter instead affecting specifically dACC. Overall, our study underscores for the first time the independent, and yet concurrent, role played by two different facets of human executive functions in the neural response to pain.

References

Atlas, L.Y., Bolger, N., Lindquist, M.A., et al. (2010). Brain mediators of predictive cue effects on perceived pain. *The Journal of Neuroscience*, **30**, 12964–77

Buhle, J., Wager, T.D. (2010). Performance-dependent inhibition of pain by an executive working memory task. *Pain*, **149**, 19–26

Bushnell, M.C., Čeko, M., Low, L.A. (2013). Cognitive and emotional control of pain and its disruption in chronic pain. *Nature Reviews Neuroscience*, **14**, 502–11

Duker, P.C., van den Bercken, J., Foekens, M.-A. (1999). Focusing versus distraction and the response to clinical electric shocks. *Journal of Behavior Therapy and Experimental Psychiatry*, **30**, 199–204

Fan, L., Li, H., Zhuo, J., et al. (2016). The Human Brainnetome Atlas: A New Brain Atlas Based on Connectional Architecture. *Cerebral Cortex*, **26**, 3508–26

Fazeli, S., Büchel, C. (2018). Pain-Related Expectation and Prediction Error Signals in the Anterior Insula Are Not Related to Aversiveness. *Journal of Neuroscience*, **38**, 6461–74

Friston, K.J., Worsley, K.J., Frackowiak, R.S.J., et al. (1993). Assessing the significance of focal activations using their spatial extent. *Human Brain Mapping*, **1**, 210–20

Geuter, S., Boll, S., Eippert, F., et al. (2017). Functional dissociation of stimulus intensity encoding and predictive coding of pain in the insula. *eLife*, **6**

Hodes, R.L., Rowland, E.W., Lightfoot, N., et al. (1990). The effects of distraction on responses to cold pressor pain. *Pain*, **41**, 109–14

Hoegh, M., Seminowicz, D.A., Graven-Nielsen, T. (2019). Delayed effects of attention on pain sensitivity and conditioned pain modulation. *European Journal of Pain*, **23**, 1850–62

Hung, Y., Gaillard, S.L., Yarmak, P., et al. (2018). Dissociations of cognitive inhibition, response inhibition, and emotional interference: Voxelwise ALE meta-analyses of fMRI studies. *Human Brain Mapping*, **39**, 4065–82

Keogh, E., Hatton, K., Ellery, D. (2000). Avoidance versus focused attention and the perception of pain: differential effects for men and women. *Pain*, **85**, 225–30

Kragel, P.A., Kano, M., Oudenhove, L.V., et al. (2018). Generalizable representations of pain, cognitive control, and negative emotion in medial frontal cortex. *Nature Neuroscience*, **21**, 283

Laird, A.R., McMillan, K.M., Lancaster, J.L., et al. (2005). A comparison of label-based review and ALE meta-analysis in the Stroop task. *Human Brain Mapping*, **25**, 6–21

Legrain, V., Damme, S.V., Eccleston, C., et al. (2009). A neurocognitive model of attention to pain: behavioral and neuroimaging evidence. *Pain*, **144**, 230–32

McCaul, K.D., Monson, N., Maki, R.H. (1992). Does distraction reduce pain-produced distress among college students? *Health Psychology*, **11**, 210–17

McLaren, D.G., Ries, M.L., Xu, G., et al. (2012). A generalized form of context-dependent psychophysiological interactions (gPPI): A comparison to standard approaches. *NeuroImage*, **61**, 1277–86

Nouwen, A., Cloutier, C., Kappas, A., et al. (2006). Effects of focusing and distraction on cold pressor-induced pain in chronic back pain patients and control subjects. *The Journal of Pain*, **7**, 62–71

Petrovic, P., Petersson, K.M., Ghatan, P.H., et al. (2000). Pain-related cerebral activation is altered by a distracting cognitive task. *Pain*, **85**, 19–30

Riontino, L., Fournier, R., Lapteva, A., et al. (2022). Cognitive exertion affects the appraisal of one's own and other people's pain. *bioRxiv*

Seminowicz, D.A., Davis, K.D. (2007a). A re-examination of pain–cognition interactions: Implications for neuroimaging. *PAIN*, **130**, 8–13

Seminowicz, D.A., Davis, K.D. (2007b). Interactions of Pain Intensity and Cognitive Load: The Brain Stays on Task. *Cerebral Cortex*, **17**, 1412–22

Seminowicz, D.A., Mikulis, D.J., Davis, K.D. (2004). Cognitive modulation of pain-related brain responses depends on behavioral strategy. *Pain*, **112**, 48–58

Shackman, A.J., Salomons, T.V., Slagter, H.A., et al. (2011). The integration of negative affect, pain and cognitive control in the cingulate cortex. *Nature Reviews. Neuroscience*, **12**, 154–67

Sharvit, G., Corradi-Dell'Acqua, C., Vuilleumier, P. (2018). Modality-specific effects of aversive expectancy in anterior insula and medial prefrontal cortex. *Pain*, **159**, 1529–42

Sharvit, G., Lin, E., Vuilleumier, P., et al. (2020). Does inappropriate behavior hurt or stink? The interplay between neural representations of somatic experiences and moral decisions. *Science Advances*, **6**

Silvestrini, N., Chen, J.-I., Piché, M., et al. (2020). Distinct fMRI patterns colocalized in the cingulate cortex underlie the after-effects of cognitive control on pain. *NeuroImage*, **217**, 116898

Silvestrini, N., Corradi-Dell'Acqua, C. (2022). The Impact of Pain on Subsequent Effort and Cognitive Performance. *Journal of Psychophysiology*

Silvestrini, N., Rainville, P. (2013). After-effects of cognitive control on pain. *European Journal of Pain*, **17**, 1225–33

Sprenger, C., Finsterbusch, J., Büchel, C. (2015). Spinal Cord–Midbrain Functional Connectivity Is Related to Perceived Pain Intensity: A Combined Spino-Cortical fMRI Study. *Journal of Neuroscience*, **35**, 4248–57

Tinnermann, A., Geuter, S., Sprenger, C., et al. (2017). Interactions between brain and spinal cord mediate value effects in nocebo hyperalgesia. *Science*, **358**, 105–8

Tracey, I., Mantyh, P.W. (2007). The cerebral signature for pain perception and its modulation. *Neuron*, **55**, 377–91

Tracey, I., Ploghaus, A., Gati, J.S., et al. (2002). Imaging Attentional Modulation of Pain in the Periaqueductal Gray in Humans. *Journal of Neuroscience*, **22**, 2748–52

Valet, M., Sprenger, T., Boecker, H., et al. (2004). Distraction modulates connectivity of the cingulo-frontal cortex and the midbrain during pain—an fMRI analysis. *Pain*, **109**, 399–408

Whitfield-Gabrieli, S., Nieto-Castanon, A. (2012). Conn: A Functional Connectivity Toolbox for Correlated and Anticorrelated Brain Networks. *Brain Connectivity*, **2**, 125–41

Wiech, K. (2016). Deconstructing the sensation of pain: The influence of cognitive processes on pain perception. *Science (New York, N.Y.)*, **354**, 584–87

Woo, C.-W., Roy, M., Buhle, J.T., et al. (2015). Distinct Brain Systems Mediate the Effects of Nociceptive Input and Self-Regulation on Pain. *PLOS Biology*, **13**, e1002036

Zalesky, A., Cocchi, L., Fornito, A., et al. (2012). Connectivity differences in brain networks. *NeuroImage*, **60**, 1055–62

Acknowledgments

NS was supported by an *Ambizione* grant awarded from the Swiss National Science Foundation (PZ00P1_142458 / 1). CCD was supported by a *Boursier* grant from the Swiss National Science Foundation (PP00P1_183715). This study was conducted at the Brain and Behavior Laboratory (BBL) at the University of Geneva and benefited from the support of the BBL technical staff.

Figure Legends

Figure 1. Behavioural responses. Boxplots and individual data describing (**A-B**) average Accuracy and correct Reaction Times associated with the Stroop Task, and (**C-D**) average Pain Intensity and Unpleasantness ratings associated with the thermal stimulations. For each boxplot, the horizontal line represents the median value of the distribution, the star represents the average, the box edges refer to the inter-quartile range, and the whiskers to the data range within 1.5 of the inter-quartile range. Individual data-points are also displayed as dots. Orange boxes and dots refer to the Stroop Interference condition (and associated thermal stimulations), whereas azure boxes/dots refer to the Stroop Neutral condition, and grey boxes/dots refer to the Baseline stimulation introducing each experimental session. "***" and "*"refer to significant condition differences at $p < 0.001$ and $p < 0.05$ respectively.

Figure 2. Stroop activity. (**A**) Surface rendering showing regions whose activity during the Stroop task increased linearly with the Reaction Times. To improve the readability of this specific plot, regions are displayed at voxel-level FWE correction for multiple comparisons for the whole brain, thus highlighting only brain portions showing the strongest association. (**B-C**) Predictions from whole brain models of Stroop demands (Silvestrini *et al.*, 2020) and pain unpleasantness (Sharvit *et al.*, 2020). Each model is described in terms of whole-brain maps with coordinates highlighted based on their relative importance. For Stroop model, coordinates describe the relative linear positive (orange) or negative (azure) contribution to the prediction. For pain unpleasantness, coordinates are coded exclusively in terms of non-linear contribution (Sharvit *et al.*, 2020). Each

model is also described in terms of its' proficiency at discriminating between Stroop trials with long vs. short response times, as displayed through dedicated boxplots. *DLPFC*: Dorsolateral Prefrontal Cortex; *AI & PI*: Anterior & Posterior Insula; *SMA*: Supplementary Motor Area; *MCC*: Middle Cingulate Cortex; *PPC*: Posterior Parietal Cortex; *pOP*: Parietal Operculum; a.u.: arbitrary units. "***" significant condition differences at $p < 0.001$.

Figure 3. Baseline temperature. (**A**) Surface rendering showing regions associated with the delivery of the baseline thermal event (when contrasted with the non-specified parts of the model [implicit baseline]). All regions displayed survive cluster-level FWE correction for multiple comparisons for the whole brain. *AI & PI*: Anterior & Posterior Insula; *pOP*: Parietal Operculum; *PPC*: Posterior Parietal Cortex; *IFG*: Inferior Frontal Gyrus (**B**) Linear regressions (with confidence interval areas) and individual data describing the predictions from whole brain models of Stroop demands (Silvestrini *et al.*, 2020) and pain unpleasantness (Sharvit *et al.*, 2020) plotted against the stimulation temperature. "*" refers to significant Pearson's r coefficient at $p < 0.05$.

Figure 4. Distraction-related activity. (**A**) Surface rendering showing regions associated with the delivery of thermal stimulation *During > After* the Stroop task. All regions displayed survive FWE correction for multiple comparisons for the whole brain at $p < 0.05$. The parameter estimates from one outlined region of interest are displayed through boxplots and individual data-points. (**B**) Connectivity changes evoked by the delivery of thermal stimulations *During vs. After* the task. Purple tracks refers to increased connectivity *During > After*, whereas green tracks refer to the opposite contrast. The connectivity parameters from the track connecting right parietal cortex to

lateral prefrontal cortex and anterior insula (*cluster 1*) are also displayed through boxplots and individual data-points. "***"refers to a significant main effect of TIMING at $p < 0.001$. *DLPFC & DMPFC*: Dorsolateral & Dorsomedial Prefrontal Cortex; *IFG*: Inferior Frontal Gyrus; *PPC*: Posterior Parietal Cortex; *MTG*: Middle Temporal Gyrus; *AI*: Anterior Insula; *ACC*: Anterior Cingulate Cortex; *TP*: Temporal pole.

Figure 5. Task-demands effects on pain activity. Surface rendering showing regions associated with the delivery of thermal stimulations associated with the *Interference > Neutral* the Stroop conditions. The activations are displayed under a threshold corresponding to $p < 0.001$ (uncorrected). The parameter estimates from the outlined region are displayed through boxplots and individual data-points. "**" and "*" refer to a significant condition differences at $p < 0.01$ and $p < 0.05$ respectively. *dACC*: dorsal Anterior Cingulate Cortex.

Figure 6. Multivariate Pattern analysis of Stroop-related pain activity. Boxplots and individual data describing the predictions from whole brain models of Stroop demands (Silvestrini *et al.*, 2020) and pain unpleasantness (Sharvit *et al.*, 2020), applied to the Stroop-related pain activity from our data. "**" and "*"refer to a significant main effect of TIMING from a Repeated Measures ANOVA at $p < 0.01$ and $p < 0.05$ respectively.

Tables

Table 1

Stroop Task: parametric modulation of Reaction Times. The implicated regions survive FWE correction for multiple comparisons at the cluster level, with an underlying voxel-level threshold corresponding to *p < 0.001*. L and R refer to the left and right hemisphere, respectively. M refers to medial activations.

	SIDE	***Coordinates***			$T_{(28)}$	***Cluster size***
		x	***y***	***z***		
Parametric modulation of Response Times						
Middle Cingulate Gyrus	M	-10	20	30	7.63	
Supplementary Motor Area	M	-4	8	50	8.78	
Precuneus	M	-10	-66	54	9.04	
Posterior Parietal Cortex	L	-38	-32	50	9.55	
Posterior Parietal Cortex	R	44	-36	42	8.71	
Anterior Insula	L	-28	22	2	10.04	
Inferior Frontal Gyrus	L	-50	12	2	6.75	
Caudate	L	-10	4	10	7.66	
Thalamus	L	-10	-18	8	8.27	
Anterior Insula	R	30	26	0	8.49	
Inferior Frontal Gyrus	R	52	12	2	6.07	73685***
Caudate	R	10	6	6	6.68	
Thalamus	R	10	-10	6	9.71	
Dorsolateral Prefrontal Cortex	R	40	36	18	7.18	
Inferior Temporal Gyrus	L	-52	-62	-8	7.85	
Inferior Temporal Gyrus	R	56	-52	-10	7.24	
Inferior Occipital Gyrus	L	-32	-86	0	6.22	
Inferior Occipital Gyrus	R	36	-88	-2	6.28	
Midbrain	M	8	-22	-12	5.78	
Cerebellum	L	-24	-70	-48	7.65	
Cerebellum	R	22	-48	-26	12.26	

*** $p < 0.001$; corrected for multiple comparisons at the cluster level for the whole brain.

Table 2

Thermal stimulations. Regions associated with the delivery of the baseline thermal event (when contrasted with the non-specified parts of the model [implicit baseline]), and with the main effect of TIMING (during > after). All regions, survive FWE correction for multiple comparisons at the cluster level, with an underlying voxel-level threshold corresponding to *p < 0.001*.

	SIDE	***Coordinates***			***$T_{(28)}$***	***Cluster size***
		x	***y***	***z***		
Baseline Thermal Stimulation						
Posterior Insula	L	-30	-18	12	5.75	2175***
Anterior Insula	L	-30	6	12	6.97	
Posterior Insula	R	42	-4	0	5.90	
Anterior Insula	R	38	18	-6	8.20	
Inferior Frontal Gyrus	R	44	46	2	6.24	4408***
Pallidum	R	18	4	-4	4.47	
Caudate	R	16	16	12	4.31	
Posterior Parietal Cortex	L	-58	-42	48	7.03	547**
Parietal Operculum	L	-64	-26	22	4.95	
Posterior Parietal Cortex	R	62	-36	46	5.89	595**
Parietal Operculum	R	56	-26	24	5.27	
TIMING main effect: during > after						
Dorsolateral Prefrontal Cortex	L	-36	18	46	6.84	1466***
Dorsolateral Prefrontal Cortex	R	40	22	32	5.24	527**
Dorsomedial Prefronal Cortex	M	-2	44	30	4.30	345*
Posterior Parietal Cortex	L	-60	-50	36	4.24	
Superior Temporal Gyrus	L	-46	-48	20	5.97	1837***
Middle Temporal Gyrus (*post. part*)	L	-58	-38	-4	7.62	
Superior Temporal Gyrus	R	62	-50	14	5.23	
Middle Temporal Gyrus (*post. part*)	L	54	-28	-6	5.14	700**
Middle Temporal Gyrus *(ant. part)*	R	52	-4	-22	6.02	
Inferior Occipital Gyrus	L	-24	-98	0	14.47	
Inferior Temporal Gyrus	L	-44	-56	-14	5.33	1640***
Cerebellum	L	-20	-84	-32	5.51	
Inferior Occipital Gyrus	R	26	-96	0	9.51	501**

*** $p < 0.001$; ** $p < 0.01$; *$p < 0.05$ corrected for multiple comparisons at the cluster level for the whole brain.

Table 3

ROI-to-ROI connectivity analysis. Change of functional connectivity associated with the main effect of TIMING. The implicated tracks survive Spatial Pairwise Clustering for multiple comparisons (Zalesky *et al.*, 2012). Each cluster, is described in terms of contributing paths, t-test statistic, and global Mass index. The name of each region is drawn from the Brainnectome atlas (Fan et al., 2016, Table 1).

Connection	$T_{(28)}$	Mass
R IFJ → R SPL A7r	-4.78***	184.31
R SPL A7c → R STG A38l	-4.65***	
R SPL A7r → R IFG A44d	-4.40***	
R SPL A7r → R IFJ	-3.83***	
R IFG A44d → R SPL A5l	-3.58***	
R SPL A5l → R IFG A44d	-3.56**	
R STG A38l → R SPL A7c	-3.54**	
R SPL A7c → R IFG A44d	-3.49**	
R SPL A7r → R STG A38l	-3.39**	
R IFG A44d → R SPL A7r	-3.39**	
R SPL A7r → R vAI	-3.01**	
R SPL A7c → R IFJ	-2.80**	
R IFG A44d → R SPL A7c	-2.80**	
R IFJ → R SPL A7c	-2.80**	
L SPL A7r → R IFG A44d	-5.05***	154.59
R IFG A44d → L SPL A7r	-3.74***	
L SPL A7r → R IFJ	-3.56**	
L SPL A5l → R IFJ	-3.41**	
R IFG A44d → L SPL A5l	-3.35**	
R IFG A44d → L SPL A7ip	-3.30**	
L SPL A5l → R IFG A44d	-3.31**	
L SPL A7ip → R IFG A44d	-3.27**	
L SPL A7c → R IFJ	-3.21**	
L SPL A7c → R IFG A44d	-3.18**	
R IFJ → R IFG A44d	-3.10**	
R IFJ → L SPL A7c	-2.93**	
R IFG A44d → L SPL A7c	-2.27**	
R IFG A44d → L ACC A32p	4.07***	147.84
L ACC A32p → R IFG A44d	3.98***	
R IFJ → L ACC A32sg	3.88***	
L ACC A32p → R IFJ	3.86***	
R IFG A44d → L ACC A32sg	3.45**	
R IFJ → L ACC A32p	3.43**	
R IFJ → R ACC A24rv	3.30**	
R IFJ → R ACC A32sg	3.30**	
R IFG A45c → L ACC A32p	3.26**	
L ACC A32p → R IFG A45c	3.25**	
R IFG A45c → L ACC A32sg	3.19**	
R ACC A32sg → R IFJ	2.98**	

Figures

Figure 1

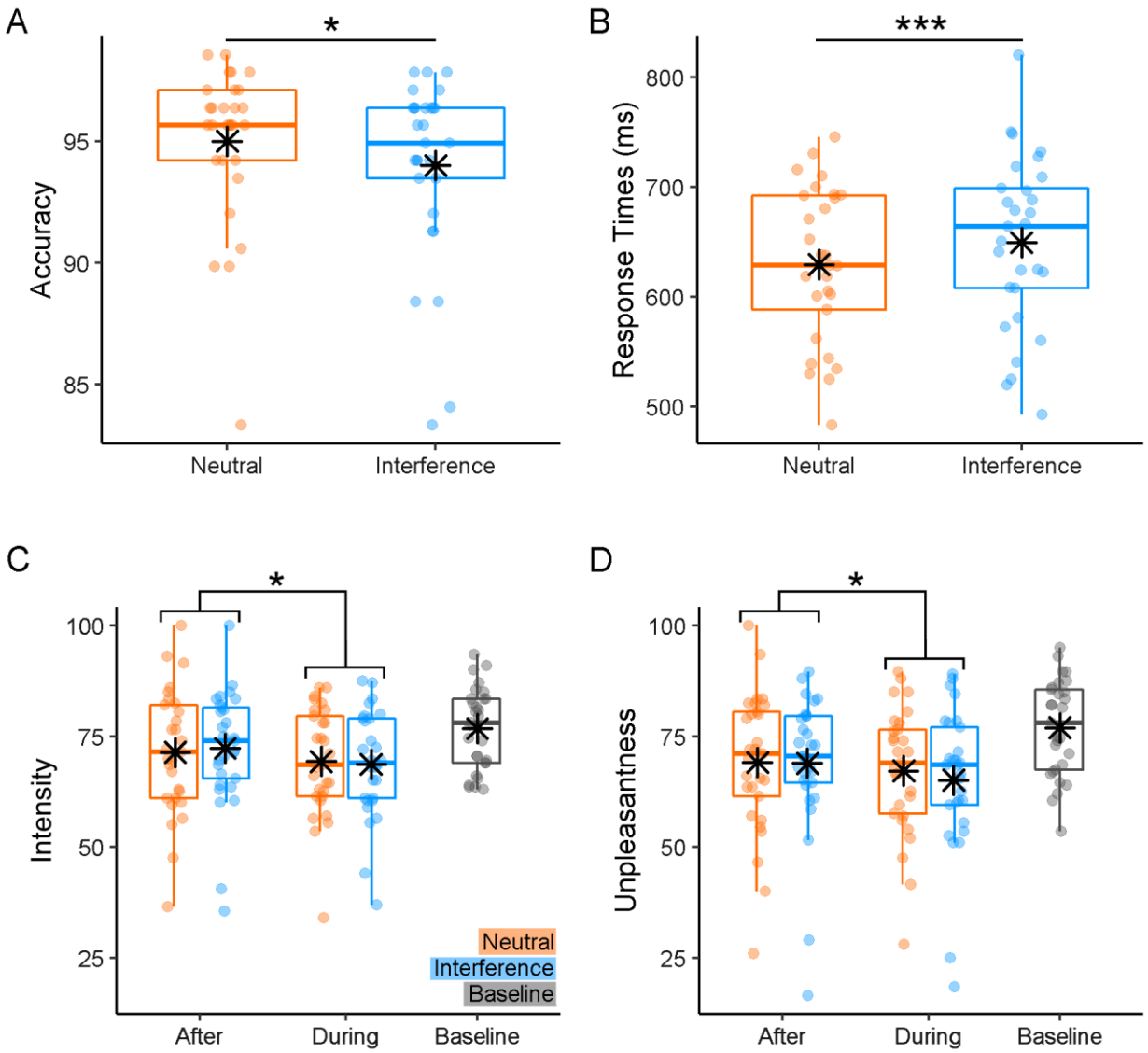

Figure 2

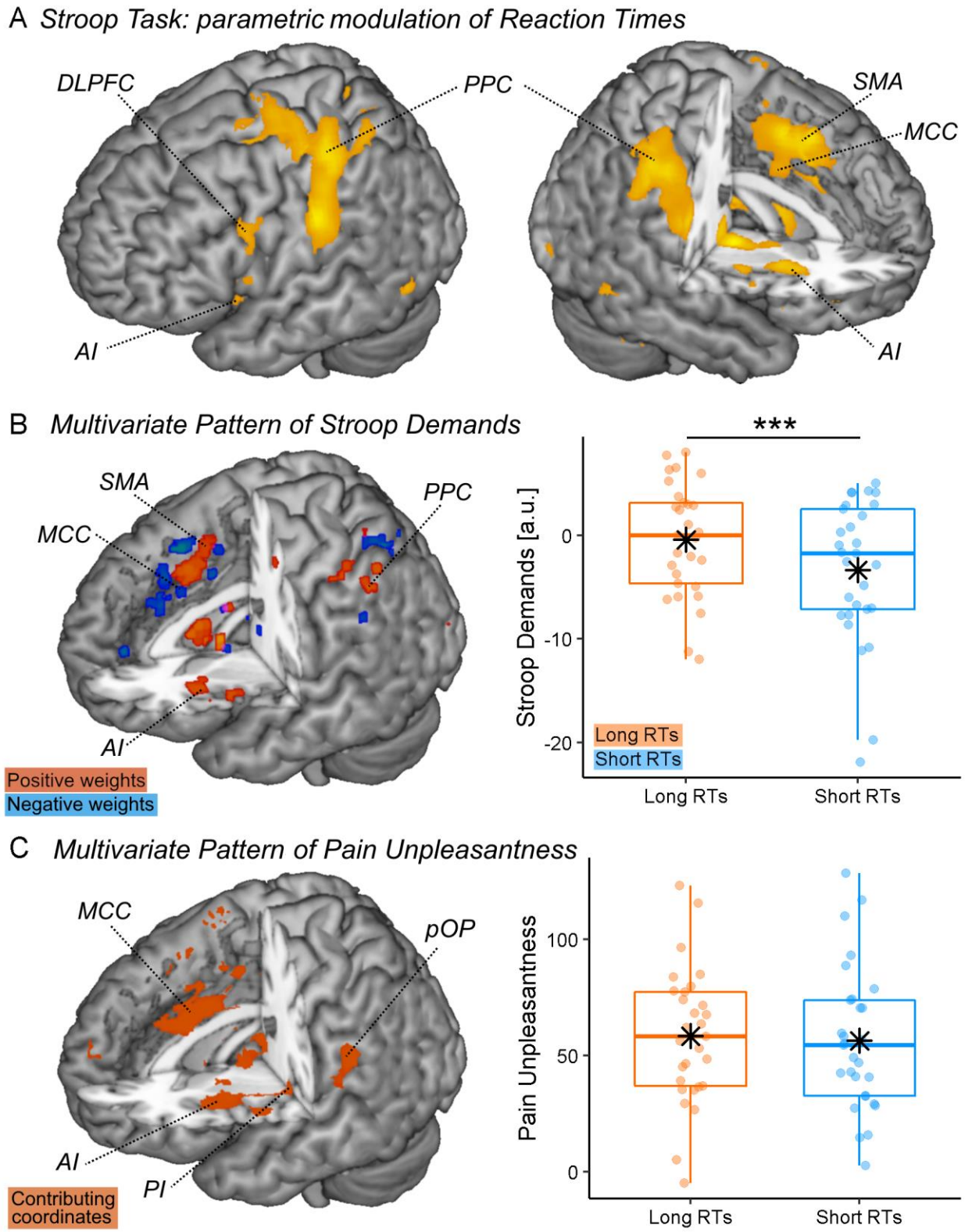
A Stroop Task: parametric modulation of Reaction Times
DLPFC
PPC
SMA
MCC
AI
AI
B Multivariate Pattern of Stroop Demands
SMA
PPC
MCC
AI
Positive weights
Negative weights
***
Stroop Demands [a.u.]
0
-10
-20
Long RTs
Short RTs
Long RTs
Short RTs
C Multivariate Pattern of Pain Unpleasantness
MCC
pOP
AI
PI
Contributing coordinates
Pain Unpleasantness
100
50
0
Long RTs
Short RTs

Figure 3

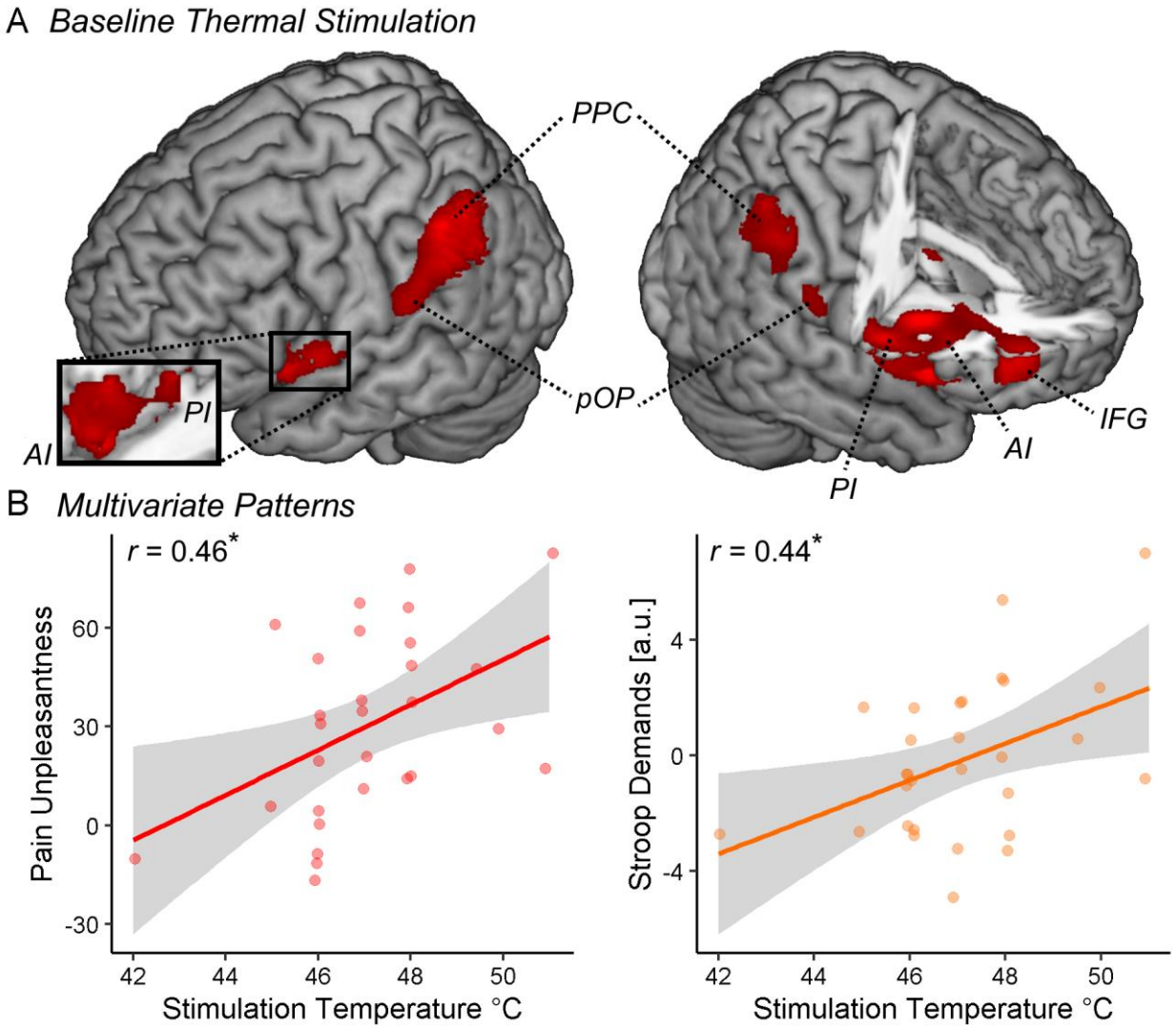
A Baseline Thermal Stimulation
PPC
pOP
PI
AI
IFG
AI
PI
B Multivariate Patterns
r = 0.46*
Pain Unpleasantness
60
30
0
-30
42
44
46
48
50
Stimulation Temperature °C
r = 0.44*
Stroop Demands [a.u.]
4
0
-4
42
44
46
48
50
Stimulation Temperature °C

Figure 4

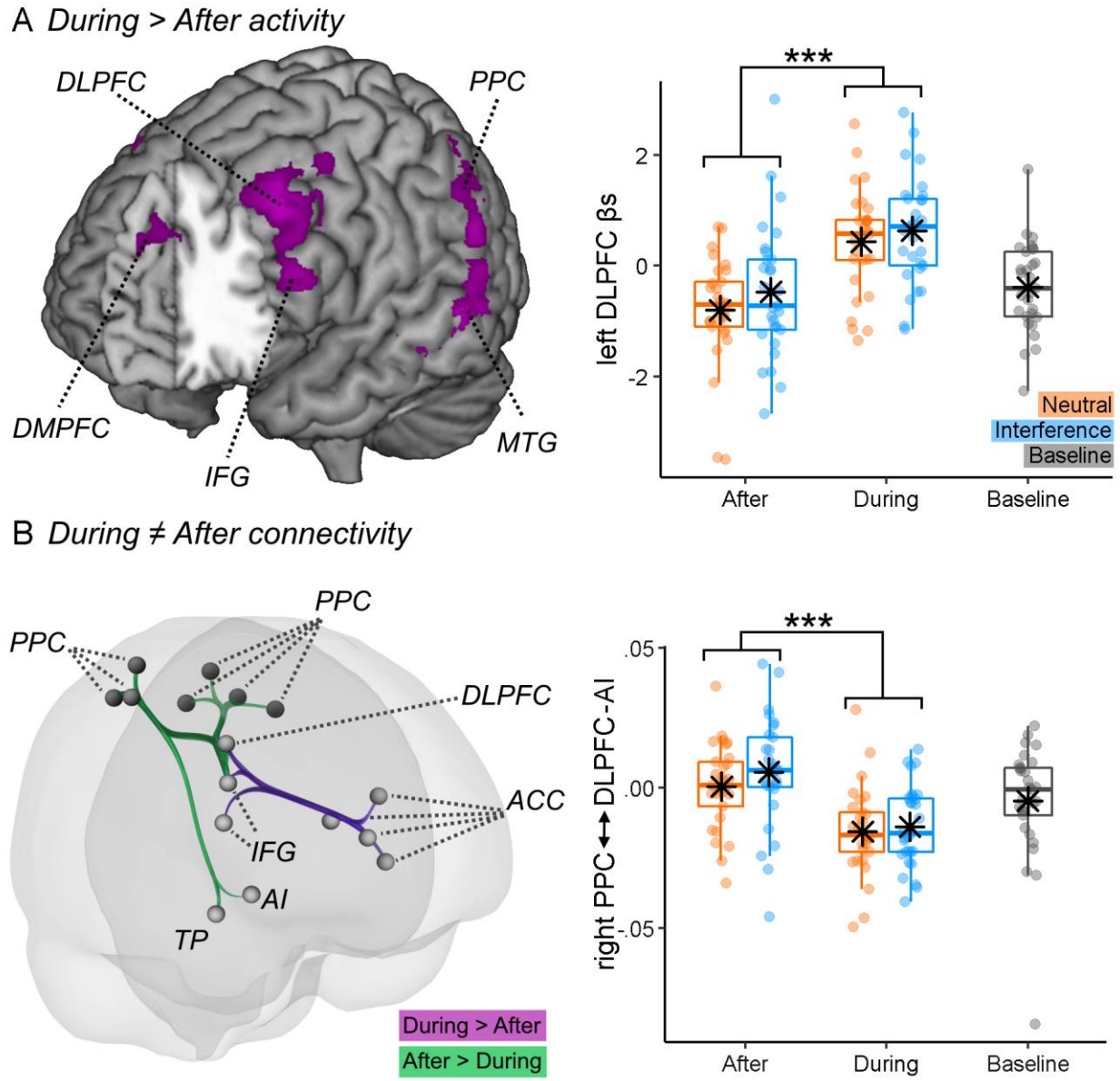
A During > After activity
DLPFC
PPC
DMPFC
IFG
MTG
***
left DLPFC βs
2
0
-2
Neutral
Interference
Baseline
After
During
Baseline
B During ≠ After connectivity
PPC
PPC
DLPFC
ACC
IFG
AI
TP
During > After
After > During
***
right PPC↔DLPFC-AI
.05
.00
-.05
After
During
Baseline

Figure 5

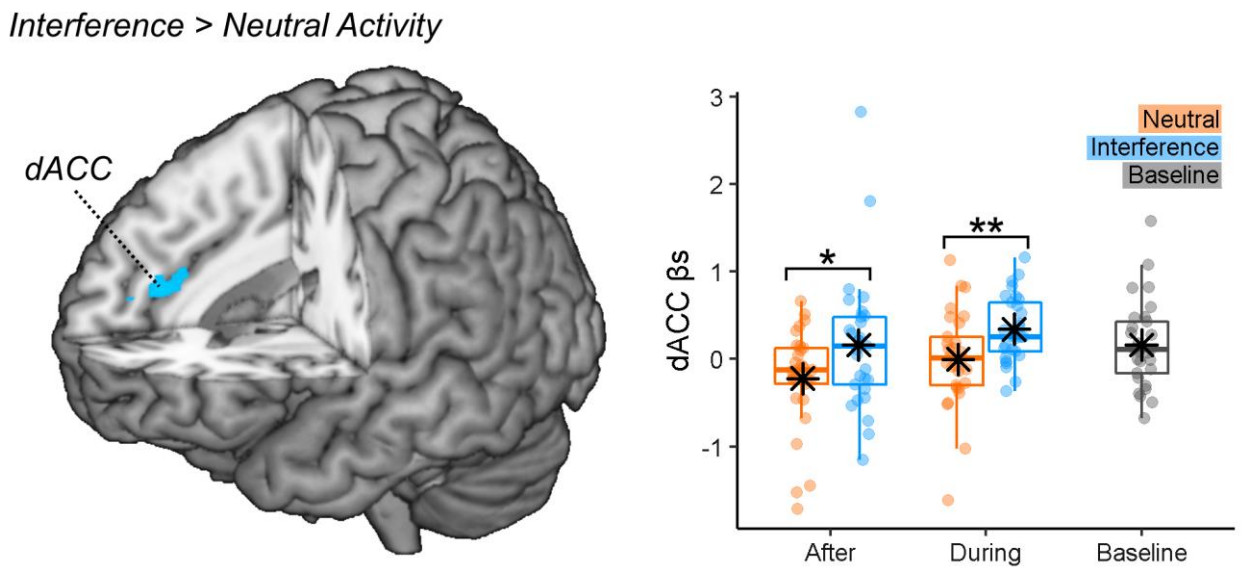
Interference > Neutral Activity
dACC
dACC βs
3
2
1
0
-1
*
**
Neutral
Interference
Baseline
After
During
Baseline

Figure 6

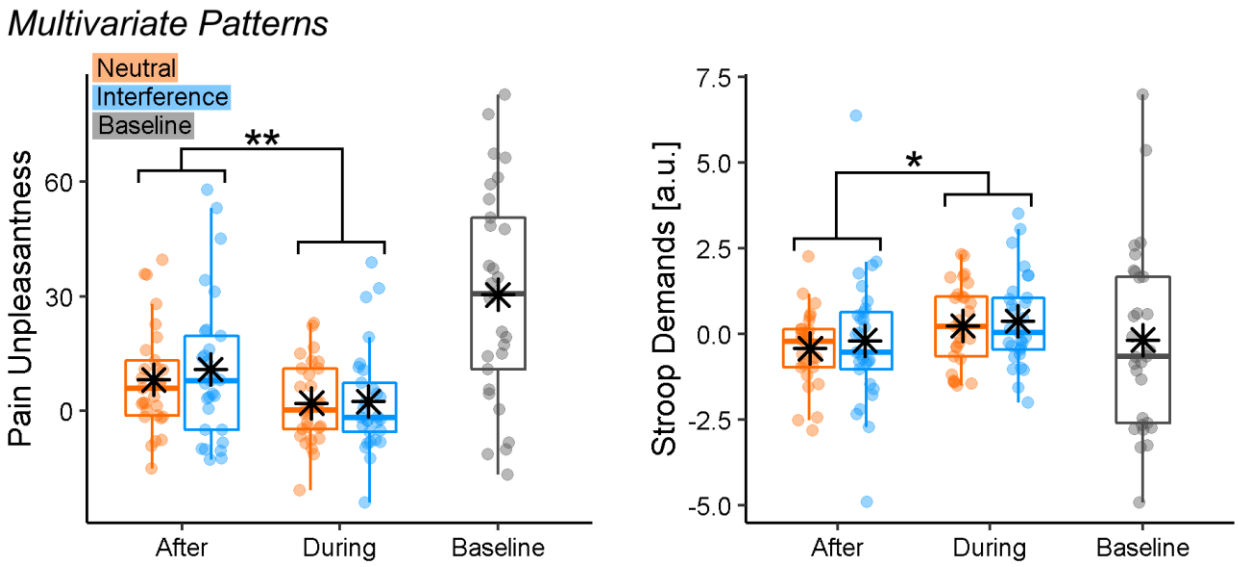
Multivariate Patterns
Neutral
Interference
Baseline
Pain Unpleasantness
60
30
0
**
After
During
Baseline
Stroop Demands [a.u.]
7.5
5.0
2.5
0.0
-2.5
-5.0
*
After
During
Baseline